



This is a repository copy of *Experimental studies of the effect of rapid afterburn on shock development of near-field explosions*.

White Rose Research Online URL for this paper:
<http://eprints.whiterose.ac.uk/108465/>

Version: Published Version

Article:

Tyas, A. orcid.org/0000-0001-6078-5215, Reay, J.J., Fay, S.D. et al. (4 more authors) (2016) Experimental studies of the effect of rapid afterburn on shock development of near-field explosions. *International Journal of Protective Structures*, 7 (3). pp. 452-465. ISSN 2041-4196

<https://doi.org/10.1177/2041419616665931>

Reuse

Items deposited in White Rose Research Online are protected by copyright, with all rights reserved unless indicated otherwise. They may be downloaded and/or printed for private study, or other acts as permitted by national copyright laws. The publisher or other rights holders may allow further reproduction and re-use of the full text version. This is indicated by the licence information on the White Rose Research Online record for the item.

Takedown

If you consider content in White Rose Research Online to be in breach of UK law, please notify us by emailing eprints@whiterose.ac.uk including the URL of the record and the reason for the withdrawal request.



eprints@whiterose.ac.uk
<https://eprints.whiterose.ac.uk/>

Experimental studies of the effect of rapid afterburn on shock development of near-field explosions

International Journal of Protective Structures
2016, Vol. 7(3) 452–465
© The Author(s) 2016
Reprints and permissions:
sagepub.co.uk/journalsPermissions.nav
DOI: 10.1177/2041419616665931
prs.sagepub.com


Andrew Tyas^{1,2}, Jonathan J Reay², Stephen D Fay^{1,2}, Samuel D Clarke,¹ Samuel E Rigby¹, James A Warren^{1,2} and Daniel J Pope³

Abstract

Many conventional high explosives do not contain sufficient internal oxygen to fully combust the gaseous products which result from detonation of the explosive material. Because of this, under-oxygenated explosives continue to burn after detonation. This process, called afterburn, is known to influence the late-time pressure and energy released by the explosive, which has particular significance for confined explosives. Recent experimental work at the University of Sheffield, along with a small number of previous studies, has shown that some afterburn occurs at timescales commensurate with the development of the shock wave. This article presents the results from a series of tests measuring the reflected pressure acting on a rigid target following the detonation of small explosive charges. High-speed video is used to capture the emerging structure of the detonation products and air shock, while the spatial and temporal distributions of the reflected pressure are recorded using an array of 17 Hopkinson pressure bars set flush with an effectively rigid target. Tests are conducted in inert atmospheres and oxygen-rich atmospheres in order to assess the contribution of rapid afterburn on the development of the shock front and interaction with a rigid target situated close to the explosive charge. The results show that early-stage afterburn has a significant influence on the reflected shock parameters in the near-field.

Keywords

Blast, experimental measurements, near-field, rapid afterburn, shock

Introduction

While the mechanisms of load transfer from high explosive (HE) blast to targets in the far-field and the magnitudes of the resulting loading are well understood, near-field HE blast has received far less attention. As a result, we are still somewhat in the dark over how the loading is generated and

¹Department of Civil and Structural Engineering, The University of Sheffield, Sheffield, UK

²Blastech Ltd, Sheffield, UK

³Defence Science and Technology Laboratory (Dstl), Salisbury, UK

Corresponding author:

A Tyas, Department of Civil and Structural Engineering, University of Sheffield, Sir Frederick Mappin Building, Mappin Street, Sheffield S1 3JD, UK.

Email: a.tyas@sheffield.ac.uk

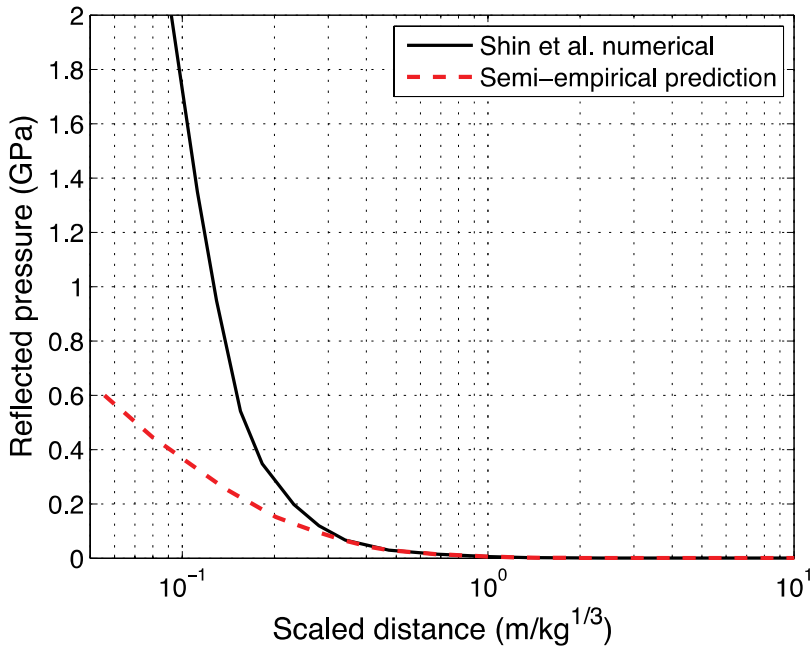


Figure 1. Predictions of near-field peak normally reflected pressure (after Shin et al. (2015)).

what the load parameters are at scaled distances $Z \ll 1 m/kg^{1/3}$. The level of uncertainty is highlighted by recent work by Shin et al. (2015), where predictions of the peak reflected pressure from numerical modelling and the well-established semi-empirical model of Kingery and Bulmash (1984) which compare very well for $Z > 1 m/kg^{1/3}$ differ by $>400\%$ at $Z = 0.1 m/kg^{1/3}$ (Figure 1).

The uncertainty over which modelling approaches are correct is due to a lack of definitive experimental data, which itself is due, in part, to the difficulty in developing accurate and robust experimental approaches to measuring loading with magnitudes in the tens, hundreds or thousands of megapascals, and with transients occurring at microsecond timescales. Experimental work on this problem can be traced back to the First World War, with the development by Bertram Hopkinson of the pressure bar that was to bear his name. Rather than the better-known use of the Hopkinson pressure bar (HPB) for dynamic characterisation of the mechanical properties of the materials, Hopkinson originally developed the HPB to study the loading from the impacts of bullets and small contact detonations on the loaded end of the bar (Hopkinson, 1914).

The modern version of the HPB, instrumented with perimeter-mounted strain gauges, is, in many respects, an excellent item of experimental equipment for measuring near-field blast loading. It is robust (able to record several hundred megapascals and survive aggressive loading environments), relatively sensitive (with care, it can differentiate pressure changes of ~ 100 kPa) and while it is well known that signals disperse as they travel from the loading face to the strain gauge recording station, the HPB still has a usable bandwidth in the range high tens to low hundreds kilohertz (Tyas and Ozdemir, 2014). It is therefore a little surprising that more use has not been made of the HPB to investigate near-field blast loading. Lee et al. (1995) used the HPB to study loading from near-field underwater detonations, while Esparza (1986, 1990) and Edwards et al. (1992) had earlier used HPBs to measure blast loading in free-air at scaled distances $Z < 0.1 m/kg^{1/3}$.

The current authors have developed an experimental facility similar to that of Esparza (Rigby et al., 2015b), but with the inclusion of high-speed video (HSV) to synchronise loading features

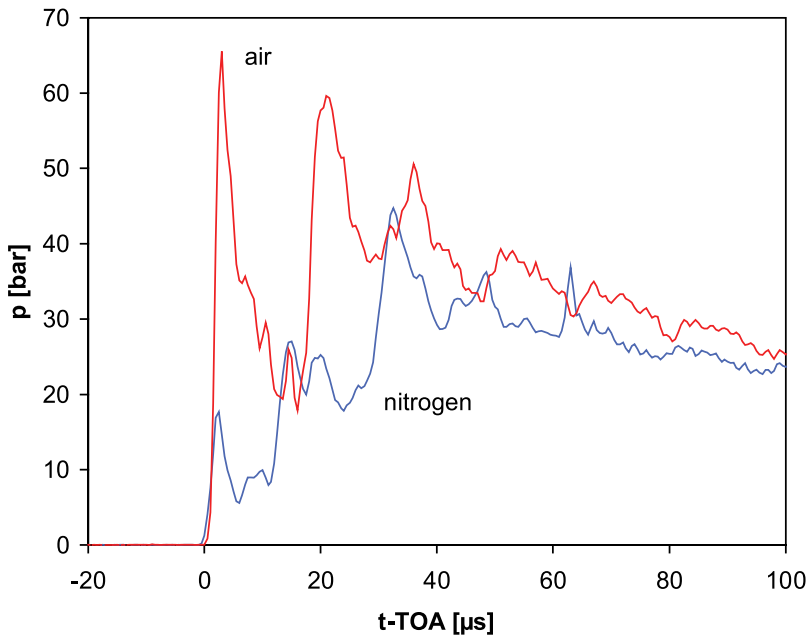


Figure 2. Experimentally recorded normally reflected shock loading of PETN spherical charges detonated in air and nitrogen.

Source: Neuwald et al. (1999).

picked up by the HPBs with physical features of the expanding detonation product cloud (DPC). This has been used to successfully record loading from small spherical Pentaerythritol tetranitrate (PETN) charges in the range $Z=0.16\text{--}0.76\text{ m/kg}^{1/3}$ (Tyas et al., 2015). This facility is termed the ‘characterisation of blast loading (CoBL)’ apparatus and the details are given in the following section.

While the foregoing work sheds some light on near-field blast loading issues, there is still much relatively unexplored on the experimental front. One important feature is the role of ‘afterburn’ in the development of near-field blast loading. It is well-known that many HE materials are fuel-rich, that is, the HE does not contain sufficient oxygen to fully oxidise the ‘fuel’ elements (mainly hydrogen and carbon) during the detonation process. The resulting DPC therefore typically contains some fraction of partially oxidised fuel which, on mixing with atmospheric oxygen at high temperature, results in energy release from a secondary reaction, or afterburn. Afterburn can release significant quantities of energy over and above that liberated by the initial detonation, and it is well established that this can contribute significantly to long-term ‘quasi-static pressure’ loading in confined explosions. It is generally considered, however, that afterburn is a relatively late-time phenomenon and does not significantly affect early-stage shock development and loading.

Neuwald et al. (1999) conducted experimental testing of sub-gram-sized charges of PETN in a small calorimeter which was filled with either air or nitrogen. They used a conventional piezoresistive pressure gauge to record the reflected pressure in the face of the calorimeter, at scaled distances of $Z\sim 1.5\text{ m/kg}^{1/3}$. They found significant reductions in the initial reflected shock loading in the inert atmosphere, with example results shown here in Figure 2.

Balakrishnan et al. (2010) conducted numerical modelling of the contribution of early-stage afterburn to the near-field blast characteristics of shock from the detonation of TNT. They noted the

importance of modelling Rayleigh–Taylor (Rayleigh, 1882; Taylor, 1950) and Richtmyer–Meshkov (Meshkov, 1969; Richtmyer, 1960) instabilities at the interface between the expanding DPC and the shocked surrounding air, since the instabilities encouraged turbulent mixing of the DPC and external oxygen and thus promoted afterburn. At $Z \sim 0.8 \text{ m/kg}^{1/3}$, they reported an increase in incident specific impulse of $\sim 60\%$ in their three-dimensional (3D) models which included this turbulent mixing, compared to one-dimensional (1D) models with no mixing at the cloud–air interface. They also noted the effect of the second shock reaching the surface of the expanding DPC in accentuating instabilities, mixing and afterburn.

This raises the issue of whether the mixing of the partially combusted DPC with the surrounding shocked air should be even more pronounced on reflection of the shock from a target surface back into the DPC in the near-field. There are two reasons to assume that this will be the case. First, the intensity of the reflected shock wave should act as a major driver of turbulent mixing. Second, the shocked air between the DPC and the target is very dense, and hence has a high spatial concentration of oxygen.

This article presents initial findings from a larger programme of experimental work conducted at the University of Sheffield to investigate this issue.

CoBL apparatus

The experimental methodology used in this work has been reported in detail in Rigby et al. (2015b) and Tyas et al. (2015), but brief details are presented here for the reader's convenience. The CoBL testing apparatus comprises a massive and stiff reaction frame, consisting of two steel fibre-and-bar-reinforced concrete portal frames spaced 1 m apart, each frame constructed from two 500 mm square cross-section columns with a 750-mm-deep, 500-mm-wide concrete beam spanning between the two columns. A 50-mm-thick steel 'acceptor' plate was cast into the underside of each of the beams to allow a 1400-mm diameter, 100-mm-thick mild steel target plate to span underneath. The entire reaction frame has a mass of around 11 tonnes. The 10-mm diameter, 3.25-m-long EN24(T) steel HPBs were inserted through tight tolerance holes at 25 mm centres on two axes centred on the centre of the target plate. The HPBs were suspended from a receiver frame placed atop the main reaction frame such that their ends sat flush with the target face. An array of 21 HPBs was used in this study; one set at the centre of the plate and four set equidistant around circumferences at 25, 50, 75 and 100 mm radial offset from the plate centre. A schematic diagram of the CoBL apparatus can be seen in Figure 3.

The explosive charge was suspended directly under the centre of the target plate on a 'drumskin' comprising a glass-fibre weave fabric (density 25 g/m^2) held taut in a steel ring, suspended, in early tests, from the target plate on adjustable screws to allow fine adjustment of the stand-off. In later tests, the drumskin was set on adjustable struts mounted in the base of the test arena.

For tests in a nitrogen atmosphere, an adjustment to the CoBL apparatus was carried out. In the revised form, a $1.5\text{-m} \times 1.5\text{-m} \times 1.5\text{-m}$ steel box was hung from the target plate with the HPBs passed through holes in the roof of the box which became the reflecting surface. The box could be purged of oxygen by slowly trickling nitrogen gas into it. The O_2 content was recorded by tapping off air from the box and passing it through an oxygen sensor. It should be noted that in these initial tests the O_2 was not completely purged due to lack of perfect sealing; there was typically $\sim 1\%–3\%$ O_2 present in the sampled atmosphere immediately prior to detonation. Video footage was obtained using a FASTCAM SA-Z high-speed digital video camera, operating at 160,000 frames per second (fps), with resolution of 384×216 pixels. An infra-red filter was used in all the tests and the tests were self-illuminated by the flash from the detonation. A sealed polycarbonate window was present in the inert atmosphere box to facilitate the video footage in those tests.

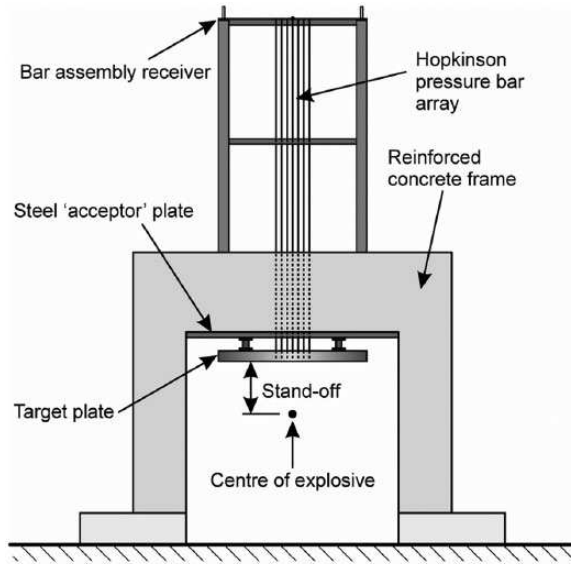


Figure 3. Schematic diagram of CoBL apparatus.

All detonations were initiated by a DynoNobel Non-electrical EX detonator, with an NEQ of 0.8 g TNT_{eq}. The detonator was placed with its tip at the centre of the spherical charge in a pre-formed hole and aligned coaxially with the normal to the target plate, with the detonator emerging from the charge on the opposite pole to the target face.

The stress pulses in the HPBs were measured using Kyowa KSP-2-120-E4 semi-conductor strain gauges, linked in such a way as to eliminate bending effects in the output strain. The strain gauge stations were mounted on the protected side of the target plate, 250 mm from the loaded faces of the HPBs and the output from the HPBs was recorded using Tie-Pie HS4 Handyscope USB digital oscilloscopes operating at 14-bit resolution and 320 ns sample rate.

Far-field blast tests – set-up and results

Prior to conducting the near-field tests, a series of small-scale open air arena tests were conducted to assess the consistency of far-field blast waves from small PETN charges. These tests were all conducted using a 0.250-kg hemispherical explosive charge, placed on small steel anvils on top of a reinforced concrete ground slab. The normally reflected pressure was recorded at gauge station G1 in Figure 4, using a Kyowa KSP piezoresistive pressure gauge mounted at the foot of, and flush with, a large reflecting wall surface, comprising a 300-mm-thick reinforced concrete bunker wall, faced with solid concrete blocks. The wall was of sufficient dimensions to render edge conditions irrelevant in the duration of the blast loading.

Six tests were conducted; two each with the explosive charge at a distance of 2, 4 and 6 m from the bunker wall. It is estimated from the results that the TNT equivalence of the PETN is 1.50, meaning that these distances correspond to $Z=2.77$, 5.55 and 8.32 m/kg^{1/3}, respectively. The results from the six tests are given in Figure 5 for pressure versus time and Figure 6 for scaled impulse versus time, that is, the temporal integral of the pressure signals divided by the cube-root of the TNT equivalent charge mass.

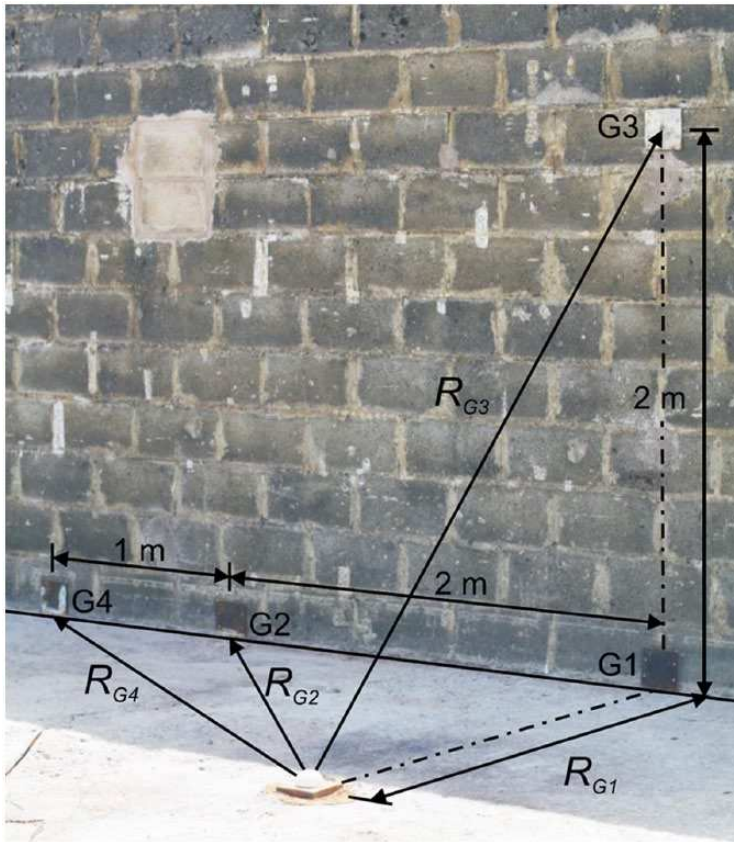


Figure 4. Set-up for far-field arena tests of hemispherical PETN charges (after Rigby et al. (2015a)).

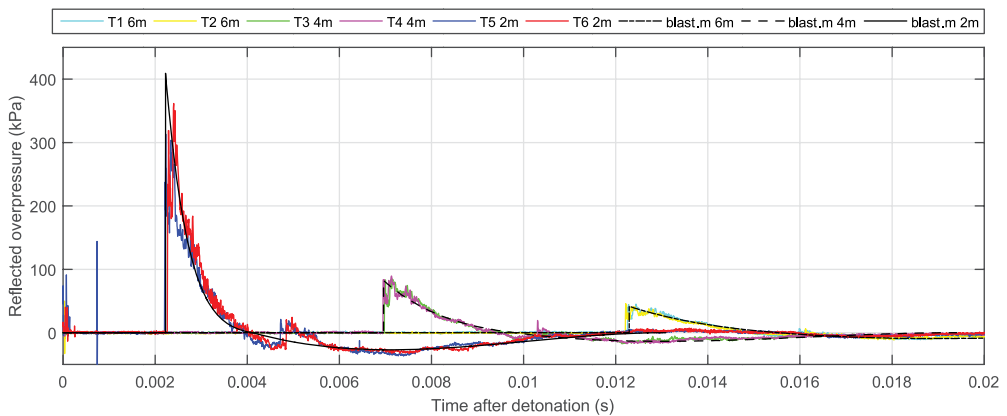


Figure 5. Normally reflected pressure versus time from free-air arena tests.

These figures also include predictions from an in-house MATLAB-based fast-running prediction code, *blast.m*, which uses the Kingery and Bulmash (1984) data for the positive phase and the

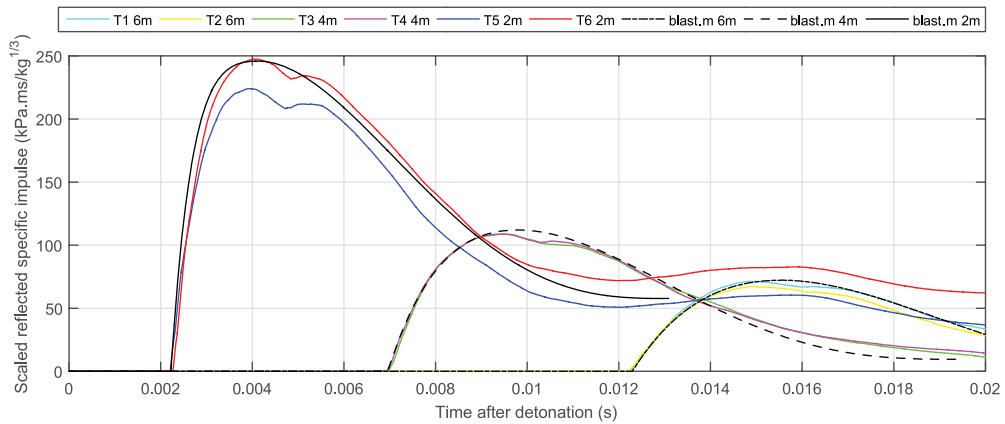


Figure 6. Scaled normally reflected specific impulse versus time from free-air arena tests.

Table 1. Near-field test programme details.

Test no.	Charge size (g TNT _{eq})	Atmosphere	O ₂ content	Stand-off (mm)	Scaled dist. (m/kg ^{1/3})
1	170	Air	20.8% (assumed)	421	0.760
2	170	Air	20.8% (assumed)	421	0.760
3	170	Air	20.8% (assumed)	421	0.760
4	170	Air	20.8% (assumed)	421	0.760
5	170	Air	20.8% (assumed)	421	0.760
6	170	Nitrogen	2.8% (measured)	421	0.760
7	170	Nitrogen	2.1% (measured)	421	0.760
8	170	Nitrogen	0.8% (measured)	421	0.760

cubic negative phase waveform proposed by Granström (1956) and recently validated by Rigby et al. (2014). The *blast.m* predictions are for 0.375 kg TNT hemispherical bursts (i.e. using a TNT equivalence factor of 1.5). The reflected pressure, specific impulse, arrival time and positive phase duration of the experimentally measured traces were quite consistent at the two larger scaled distances and correlated well with the *blast.m* predictions, until very late into the negative phase. At $Z=2.77$ m/kg^{1/3}, one experimental trace matched the *blast.m* prediction very well until close to the end of the negative phase, while the other test data generally tracked the same trend, but with a peak reflected specific impulse ~7% lower than that predicted by *blast.m* and 9% lower than the other test at this distance.

Near-field tests: results and discussion

A total of eight near-field tests were conducted as shown in Table 1. All tests were conducted with the temperature in the range 6°C–13°C and atmospheric pressure in the range 1000–1010 mb. The scaled distance of 0.760 m/kg^{1/3} was chosen as this is the range at which the shock begins to detach from the expanding DPC. Hence, at this scaled distance, the DPC had time to develop while still being close enough to the air shock front to be influenced by shock reflection from a target surface.

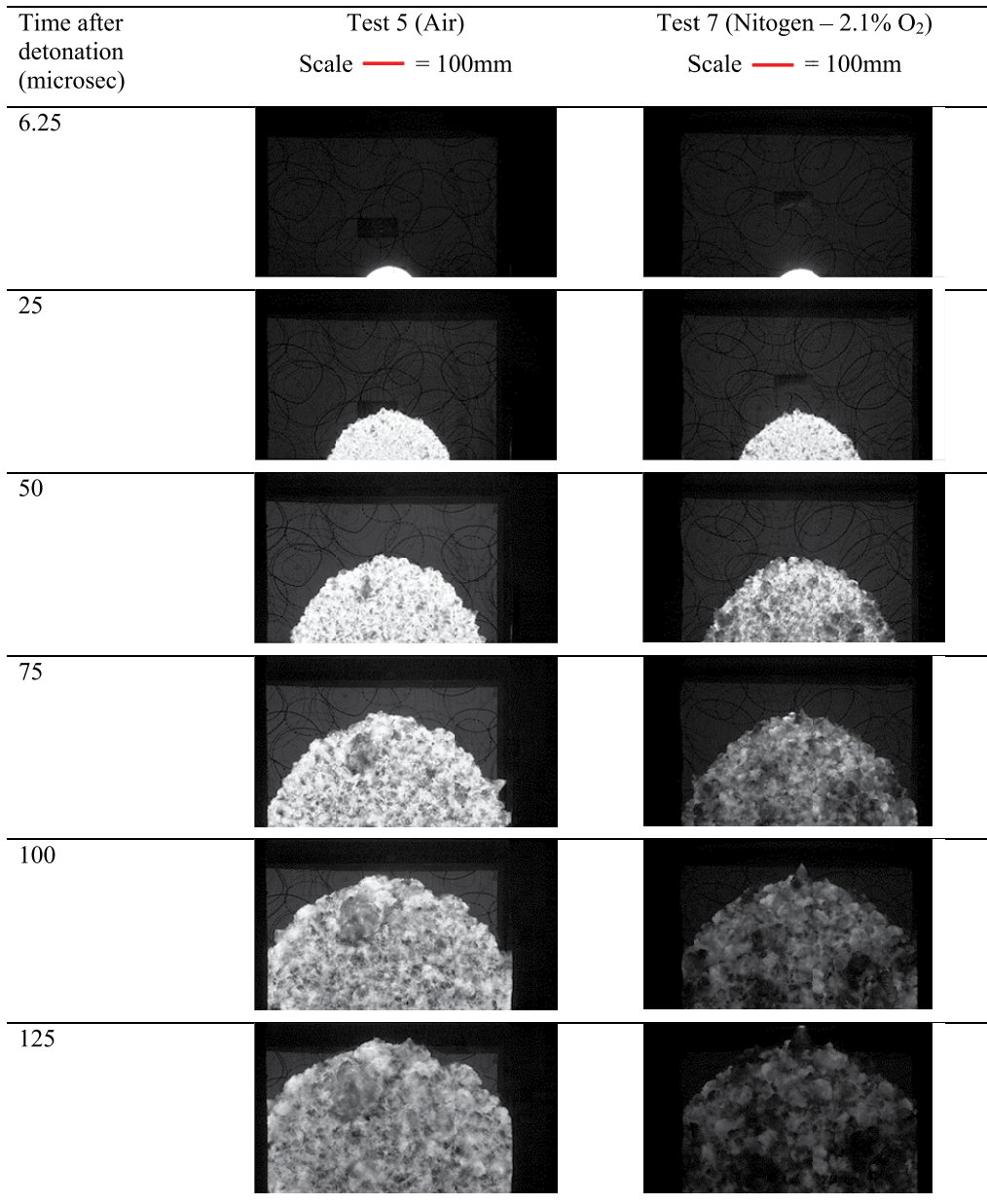


Figure 7. Still images from high-speed video footage of tests in air and nitrogen atmospheres 6.25–125 ms after detonation.

Figures 7 and 8 show stills from HSV footage of test 5 (in air) and test 7 (in nitrogen). These two tests were conducted on the same day, with identical camera placement, lenses, filters and exposure settings. The most obvious feature of these images is the dramatic reduction in incandescence of the DPC as it expands in the oxygen-poor atmosphere. It is clear that in the normal air atmosphere, oxidation and energy release is ongoing at the DPC–air interface, greatly adding to the luminosity of the DPC surface.

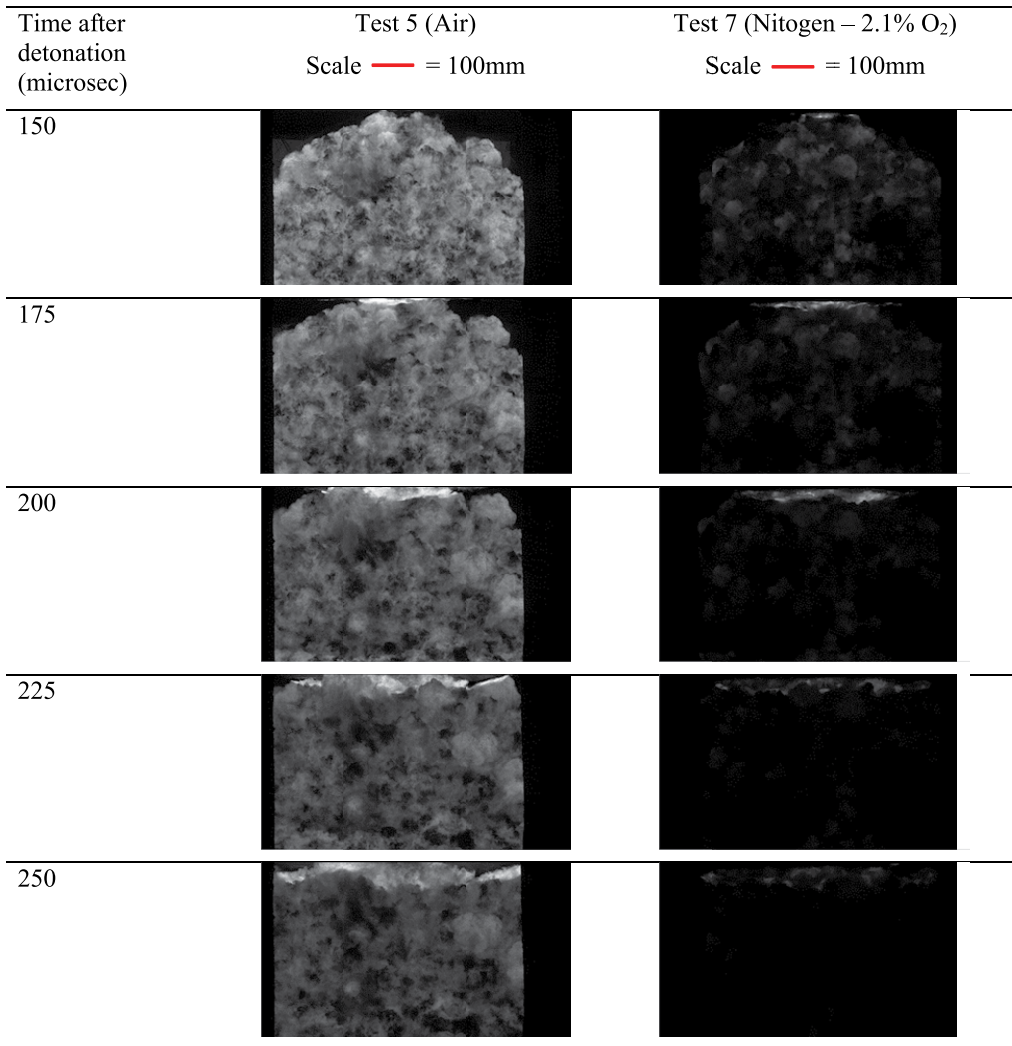


Figure 8. Still images from high-speed video footage of tests in air and nitrogen atmospheres 150–250 ms after detonation.

However, stronger afterburn in air appears to have little effect on the rate of expansion of the DPC. Figure 9 shows that there is no measurable difference in the rate of radial expansion of the front of the DPC, as measured from HSV footage from these two tests.

Closer examination of images from Figure 8 shows that as the shock front impinges on the target surface and reflects back into the DPC (from $\sim 175 \mu\text{s}$ onwards), there is a marked increase in luminosity of the DPC close to the target in air, with a still-noticeable but far less significant increase in the 2.1% O₂ atmosphere. This suggests that the afterburn is being stimulated by the turbulence generated by the shock reflection into the DPC.

Examples of data from the HPBs are shown in Figure 10, which shows, for tests 5 and 7, the central HPB and the averages of the four bars at each of the 25-mm-increment circumferences. As

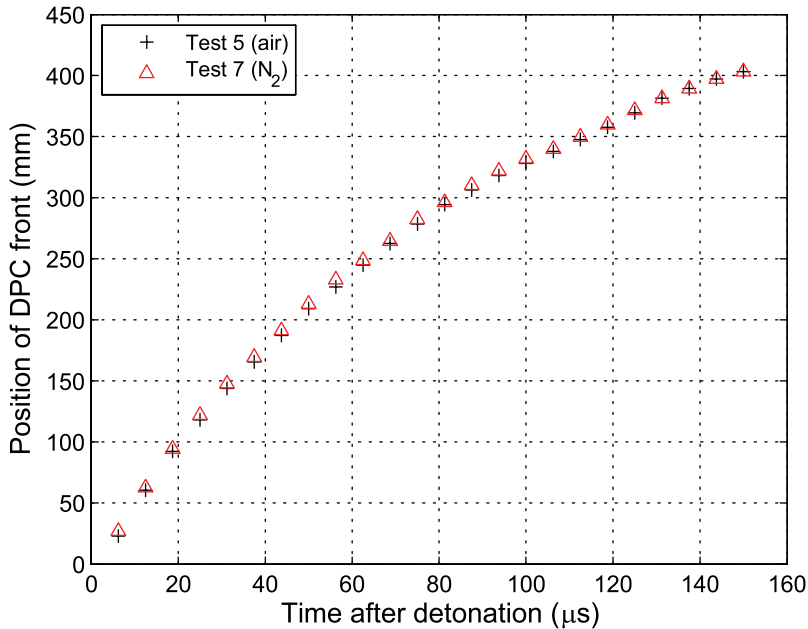


Figure 9. Expansion of detonation product cloud versus time – air and nitrogen atmospheres.

with the data in Figure 9, it is clear that the loading generally arrives at each radial offset at approximately the same time in both air and nitrogen. The exceptions to this are the results at 75 and 100 mm offset in test 7, conducted in nitrogen, where there were strong pre-cursor loading pulses in bars at 75 and 100 mm, both on the same Cartesian axis (co-axial with the view of the HSV). The pre-cursor loads on the 75 and 100 mm offset bars occurred approximately 30 and 15 μs , respectively, before the loading on the other bars at the same offsets. It is believed that these pre-cursors are due to the ‘jet’ of detonation products seen emerging from the main DPC and striking the target plate at 100–150 μs in Figure 7 and Figure 8. The nature of the jet itself is at present unclear. These jets are features regularly seen on HSV footage of these trials (e.g. just above the right horizontal in at 50–75 μs in the test 5 footage in Figure 7), although generally the jets do not strike the instrumented area of the target plate. It is possible that they are due to the inert fragments of detonator casing, with the detonator being relatively large compared to the charge in these tests. However, and interestingly, multiple similar features are present on an early-stage image from the 1985 Minor Scale detonation (Figure 11), in which the length scale of the *charge* was about 300 times greater than this work, but presumably the detonator was of a similar scale. Alternatively, the jets may be due to partially reacted material spalled from the surface of the charge by the impingement of the detonation wave, or possibly formed in a mechanism similar to shaped charge jets by the collapse of local irregularities due to Rayleigh–Taylor and Richtmyer–Meshkov instabilities on the surface of the expanding DPC.

Setting aside the issue of the jet and its associated effect on the loading, the traces on Figure 10 generally show the loading in the nitrogen atmosphere falling below that on the air atmosphere in the early stages of the decay following shock arrival. This appears to support the hypothesis that turbulent mixing due to shock reflection into the DPC is enhancing afterburn and adding to the loading in air.

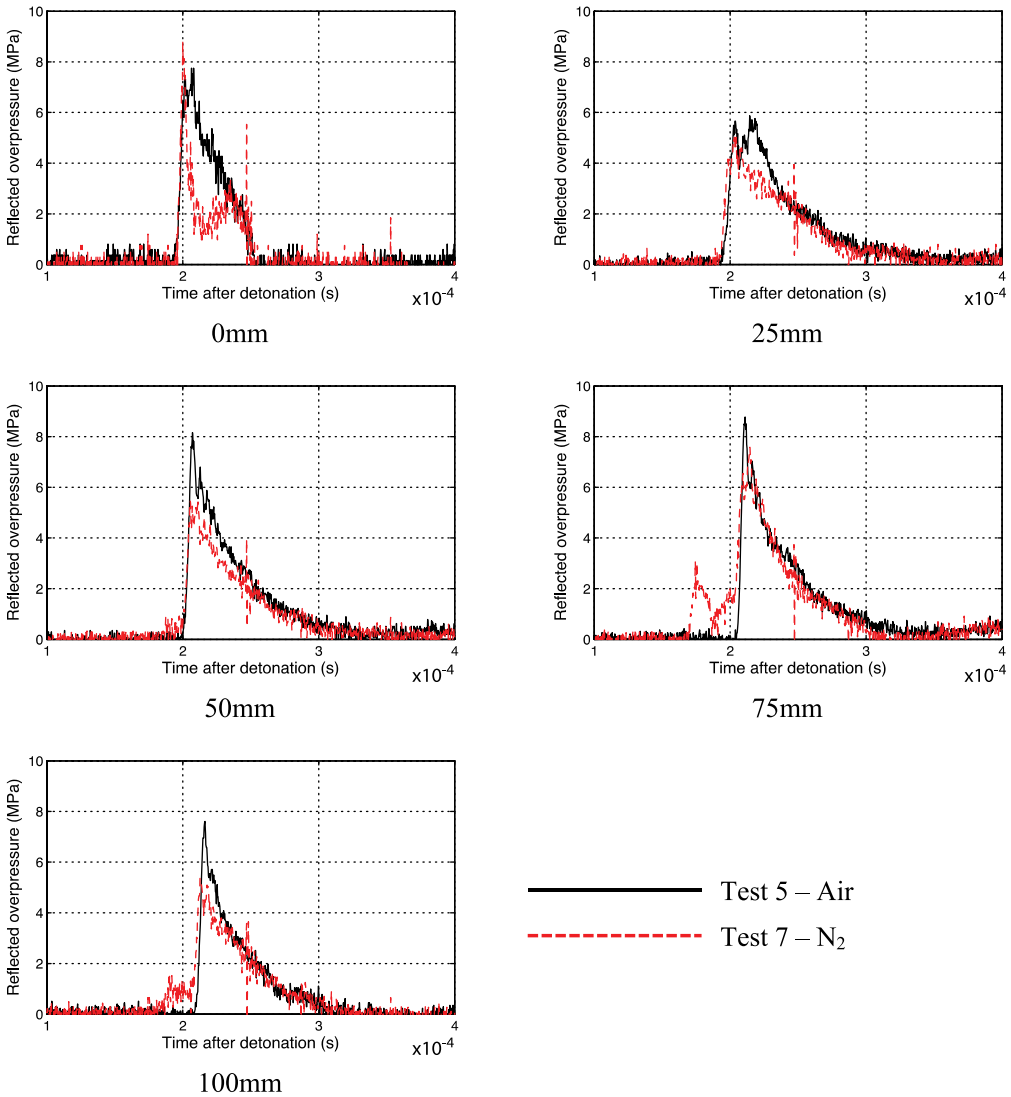


Figure 10. Examples of average pressure versus time at 0, 25, 50, 75 and 100 mm radial offset on target plate from air and nitrogen tests.

Finally, Figure 12 shows the integrated impulses from all tests conducted in this series, generated by temporally integrating the pressure–time traces up to $350\ \mu\text{s}$ after detonation (by which time the loading pulse had ended) and then spatially integrating over the annular areas between each bar radial offset. In Figure 12, the data for test 7 refer to the impulses calculated by including the pre-cursor loading pulses, while 7* refers to an estimate of the impulse with the pre-cursor loading removed, to give a better like-for-like comparison. The results are summarised in Table 2. There is a consistent reduction of loading in the nitrogen tests, with the highest value recorded in nitrogen (including the pre-cursor loading pulses) being some 6.5% lower than the lowest value in air, and the average of the values recorded in nitrogen being 15%–20% lower than the average in air.

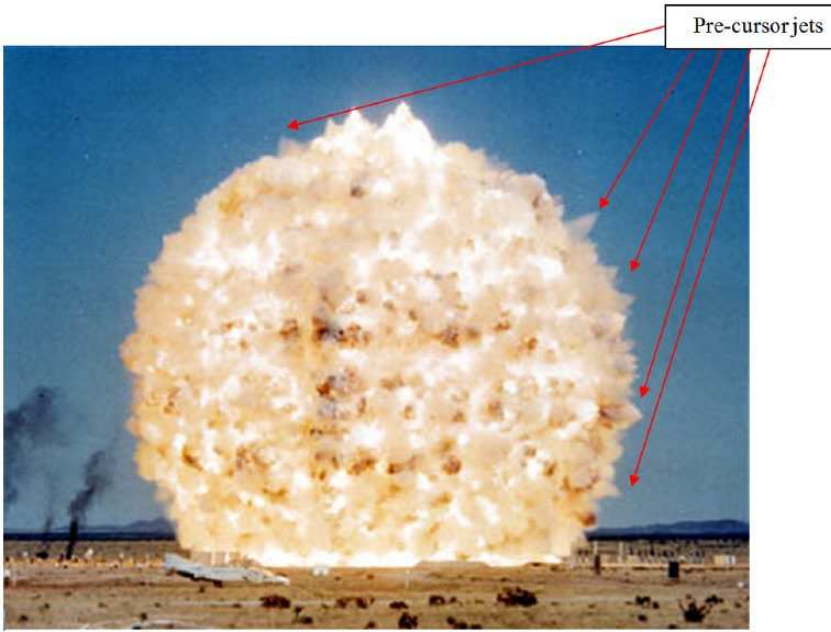


Figure 11. Detonation product cloud from 1985 Minor Scale detonation (~4500 tonnes TNT_{eq} ANFO charge).

Source: http://upload.wikimedia.org/wikipedia/commons/9/9f/Minor_Scale_test_explosion.jpg (accessed 19 July 2016).

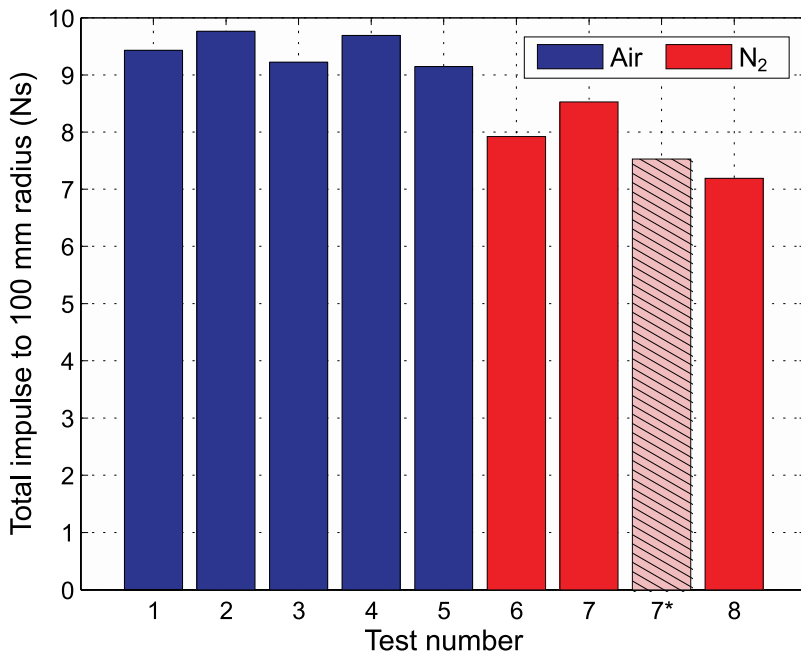


Figure 12. Total impulse recorded in air and nitrogen tests.

Table 2. Summary of impulse data.

Atmosphere	Maximum impulse (Ns)	Minimum impulse (Ns)	Average impulse (Ns)
Air	9.8	9.1	9.4
Nitrogen (including pre-cursor in test 7)	8.5	7.2	7.9
Nitrogen (not including pre-cursor in test 7)	7.9	7.2	7.5

Conclusion

Small-scale near-field tests have been conducted, of spherical PETN charges at scaled distance of $0.76 \text{ m/kg}^{1/3}$ from an instrumented target plate in both air- and oxygen-deficient atmospheres. Data from 17 HPBs set in a 100-mm-radius region around the normal between the target plate and the charge centre show a clear reduction in load of around 15%–20% in the tests conducted in nitrogen. HSV footage shows that the expanding DPC remains luminous for much longer durations in air than in nitrogen, indicating that afterburn reactions are ongoing at the cloud–air interface. However, if additional energy is being released by this mechanism, it does not appear to influence the rate of expansion of the detonation product cloud. It is tentatively hypothesised that the additional loading in air is due to a rapid afterburn due to enhanced mixing of the detonation product cloud caused by the reflection of the air shock from the target surface.

Declaration of conflicting interests

The author(s) declared no potential conflicts of interest with respect to the research, authorship and/or publication of this article.

Funding

The author(s) received no financial support for the research, authorship and/or publication of this article.

References

- Balakrishnan K, Genin F, Nance DV, et al. (2010) Numerical study of blast characteristics from detonation of homogeneous explosives. *Shock Waves* 20: 147–162.
- Edwards DH, Thomas GO, Milne A, et al. (1992) Blast wave measurements close to explosive charges. *Shock Waves* 2: 237–243.
- Esparza E (1986) Blast measurements and equivalency for spherical charges at small scaled distances. *International Journal of Impact Engineering* 4(1): 23–40.
- Esparza E (1990) Reflected blast measurements near pancake charges. In: *Proceedings of the 24th DoD explosives safety seminar*, St. Louis, MO, 28–30 August.
- Granström SA (1956) *Loading characteristics of air blasts from detonating charges*. Technical report no. 100. Stockholm: Transactions of the Royal Institute of Technology.
- Hopkinson B (1914) A method of measuring the pressure produced in the detonation of high explosives or by the impact of bullets. *Philosophical Transactions of the Royal Society Series A-Mathematical, Physical and Engineering Sciences* 213: 437–456.
- Kingery CN and Bulmash G (1984) *Airblast parameters from TNT spherical air burst and hemispherical surface burst*. Report no. ARBRL-TR-02555. Aberdeen Proving Ground, MD: U.S. Army Ballistic Research Laboratories.
- Lee C, Crawford RC, Mann KA, et al. (1995) Evidence of higher Pochhammer-Chree modes in an unsplit Hopkinson bar. *Measurement Science and Technology* 6(7): 853–859.

- Lord Rayleigh (1882) Investigation of the character of the equilibrium of an incompressible heavy fluid of variable density. *Proceedings of the London Mathematical Society* 14(1): 170–177.
- Meshkov EE (1969) Instability of the interface of two gases accelerated by a shock wave. *Fluid Dynamics* 4: 101–104.
- Neuwald P, Reichenbach H and Kuhl AL (1999) After-burning of Nitropenta products in a calorimeter. In: *17th international colloquium on dynamics of explosions and reactive systems*, Heidelberg. Available at: <http://www.iwr.uni-heidelberg.de/groups/reaflow/user/icders99/program/posters/127.pdf>
- Richtmyer RD (1960) Taylor instability in a shock acceleration of compressible fluids. *Communications on Pure and Applied Mathematics* 13: 297–319.
- Rigby SE, Fay SD, Tyas A, et al. (2015a) Angle of incidence effects on far-field positive and negative phase blast parameters. *International Journal of Protective Structures* 6(1): 23–42.
- Rigby SE, Tyas A, Bennett T, et al. (2014) The negative phase of the blast load. *International Journal of Protective Structures* 5(1): 1–20.
- Rigby SE, Tyas A, Clarke SD, et al. (2015b) Observations from preliminary experiments on spatial and temporal pressure measurements from near-field free air explosions. *International Journal of Protective Structures* 6(2): 175–190.
- Shin J, Whittaker AS and Cormie D (2015) Incident and normally reflected overpressure and impulse for detonations of spherical high explosives in free air. *ASCE Journal of Structural Engineering* 141(12)
- Taylor GI (1950) The instability of liquid surfaces when accelerated in a direction perpendicular to their planes. I. *Proceedings of the Royal Society A-Mathematical, Physical and Engineering Sciences* 201(1065): 192–196.
- Tyas A and Ozdemir Z (2014) On backward dispersion correction of Hopkinson pressure bar signals. *Philosophical Transactions of the Royal Society Series A-Mathematical, Physical and Engineering Sciences* 372.
- Tyas A, Reay JJ, Warren JA, et al. (2015) Experimental studies of blast wave development and target loading from near-field spherical PETN explosive charges. In: *16th international symposium for the interaction of the effects of munitions with structures*, Destin, FL, 9–13 November.